

1                   **Co-infection of influenza A virus enhances SARS-CoV-2 infectivity**

2   Lei Bai<sup>1,†</sup>, Yongliang Zhao<sup>1,†</sup>, Jiazhen Dong<sup>1,†</sup>, Simeng Liang<sup>1,†</sup>, Ming Guo<sup>1,†</sup>, Xinjin Liu<sup>1</sup>,  
3   Xin Wang<sup>1</sup>, Zhixiang Huang<sup>1</sup>, Xiaoyi Sun<sup>1</sup>, Zhen Zhang<sup>1</sup>, Lianghui Dong<sup>1</sup>, Qianyun Liu<sup>1</sup>,  
4   Yucheng Zheng<sup>1</sup>, Danping Niu<sup>1</sup>, Min Xiang<sup>1</sup>, Kun Song<sup>1</sup>, Jiajie Ye<sup>1</sup>, Wenchao Zheng<sup>1</sup>,  
5   Zhidong Tang<sup>1</sup>, Mingliang Tang<sup>1</sup>, Yu Zhou<sup>1</sup>, Chao Shen<sup>1</sup>, Ming Dai<sup>3</sup>, Li Zhou<sup>1</sup>, Yu Chen<sup>1</sup>,  
6   Huan Yan<sup>1</sup>, Ke Lan<sup>1,2,3,\*</sup> and Ke Xu<sup>1,\*</sup>

7

8   <sup>1</sup>State Key Laboratory of Virology, College of Life Sciences, Wuhan University, Wuhan  
9   430072, P.R. China

10   <sup>2</sup>Frontier Science Center for Immunology and Metabolism, Wuhan University, Wuhan  
11   430072, P.R. China

12   <sup>3</sup>Animal Biosafety Level 3 Laboratory, Wuhan University, Wuhan 430072, P.R. China

13

14   \*Corresponding authors. Address correspondence and reprint requests to Dr. Ke Xu (E-  
15   mail: [xuke03@whu.edu.cn](mailto:xuke03@whu.edu.cn), Tel: 86-27-68756997, Fax: 86-27-68754592) and Dr. Ke Lan  
16   (E-mail: [klan@whu.edu.cn](mailto:klan@whu.edu.cn), Tel: 86-27- 68788897, Fax: 86-27-68754592)

17

18   <sup>†</sup>These authors contributed equally to this work.

19 **Abstract**

20 The upcoming flu season in the northern hemisphere merging with the current COVID-19  
21 pandemic raises a potentially severe threat to public health. Through experimental co-  
22 infection of IAV with either pseudotyped or SARS-CoV-2 live virus, we found that IAV  
23 pre-infection significantly promoted the infectivity of SARS-CoV-2 in a broad range of cell  
24 types. Remarkably, increased SARS-CoV-2 viral load and more severe lung damage were  
25 observed in mice co-infected with IAV *in vivo*. Moreover, such enhancement of SARS-  
26 CoV-2 infectivity was not seen with several other viruses probably due to a unique IAV  
27 segment as an inducer to elevate ACE2 expression. This study illustrates that IAV has a  
28 special nature to aggravate SARS-CoV-2 infection, and prevention of IAV is of great  
29 significance during the COVID-19 pandemic.

## 30 **Introduction**

31 The outbreak of Severe Acute Respiratory Syndrome Coronavirus 2 (SARS-CoV-2) at  
32 the end of 2019 has become pandemic worldwide. Up to date, there had been more than 36  
33 million confirmed infected cases and 1 million deaths globally (<https://covid19.who.int/>).  
34 The ending time and the final severity of the current COVID-19 pandemic wave are still  
35 uncertain. Meanwhile, the upcoming seasonal influenza merging with the current pandemic  
36 might bring more challenges and pose a bigger threat to public health. There are many  
37 debates on whether seasonal flu would impact the severity of the COVID-19 pandemic and  
38 whether massive influenza vaccination is necessary for the coming winter. However, no  
39 experimental evidence is available concerning IAV and SARS-CoV-2 co-infection.

40 It is well known that disease symptoms from SARS-CoV-2 and IAV infections are quite  
41 similar, such as fever, cough, pneumonia, acute respiratory distress syndrome, etc(1, 2).  
42 Moreover, both SARS-CoV-2 and IAV are airborne transmitted pathogens that infect the  
43 same human tissues such as the respiratory tract, nasal, bronchial, and alveolar epithelial  
44 cultures(3, 4). Besides, alveolar type II cells (AT2 pneumocytes) appeared to be  
45 preferentially infected by SARS-CoV-2, which were also the primary site of IAV  
46 replication(5, 6). Therefore, the overlap of the COVID-19 pandemic and seasonal influenza  
47 would pose a large population under the high risks of co-occurrent infection by these two  
48 viruses(7).

49 Unfortunately, during the last winter flu season in the southern hemisphere, there was  
50 little epidemiological evidence about the interaction between COVID-19 and flu, probably

51 due to a low IAV infection rate resulted from social distancing(8, 9). A case report showed  
52 that three out of four SARS-CoV-2 and IAV co-infected patients rapidly develop to  
53 respiratory deterioration(10). On the contrary, other reports only observed mild symptoms  
54 in limited co-infection outpatients(11). Thus, the clinical co-infection outcomes are still  
55 unclear when a large population will face the threats of both viruses.

56 In this study, we tested whether IAV infection could affect the subsequent SARS-CoV-2  
57 infection in both infected cells and mice. The results demonstrate that the pre-infection of  
58 IAV strongly enhances the infectivity of SARS-CoV-2 by boosting viral entry in the cells  
59 and by elevating viral load plus more severe lung damage in infected mice. These data  
60 suggest a clear auxo-action of IAV on SARS-CoV-2 infection, which implies the great  
61 importance of influenza virus and SARS-CoV-2 co-infection to public health.

## 62 **Results**

### 63 **IAV promotes SARS-CoV-2 virus infectivity.**

64 To study the interaction between IAV and SARS-CoV-2, A549 (a hypotriploid alveolar  
65 basal epithelial cell line) cells that are susceptible to IAV infection but usually do not  
66 support SARS-CoV-2 infection were applied to test whether IAV pre-infection would  
67 modulate the infectivity of SARS-CoV-2. Pseudotyped VSV luciferase-reporter particles  
68 bearing SARS-CoV-2 spike protein (pSARS-CoV-2) were used to reflect the virus entry  
69 activity(12). The cells were firstly infected with IAV (A/WSN/1933[H1N1]) or mock-  
70 infected for 6 h, 12 h, or 24 h respectively, and then infected with the pSARS-CoV-2 virus  
71 for another 24 h (experimental scheme shown in Fig.1A). The data in Fig. 1B showed that  
72 A549 was converted to be highly sensitive (up to 10,000-fold) against the pSARS-CoV-2  
73 virus after different doses of IAV infections (from low MOI of 0.01 to high MOI of 1, also  
74 shown by pSARS-CoV-2 with mCherry reporter in Fig. S1). In contrast, the pre-infection  
75 of IAV had no impacts on pseudotyped VSV particles bearing VSV-G protein (Fig.1C). We  
76 further tested more cell lines to show that the enhancement of the pSARS-CoV-2 infectivity  
77 by IAV was a general effect although the increased folds were different (lower basal level  
78 of infectivity, higher enhancement fold) (Fig.1D).

79 To validate the above results, we substituted the pSARS-CoV-2 with the SARS-CoV-2  
80 live (experimental scheme shown in Fig.1E). We found that the pre-infection of IAV  
81 strongly increased the copy numbers of the SARS-CoV-2 genome (E and N genes) in both  
82 cell lysates and supernatants of A549 (~15 folds) (Fig.1F). Notably, in Calu-3 (Fig.1G) and

83 NHBE (Fig.1H) cells that are initially susceptible to SARS-CoV-2, IAV pre-infection could  
84 further increase >5 folds of SARS-CoV-2 infectivity.

85 Collectively, these data suggest an auxo-action of IAV on SARS-CoV-2 in a broad range  
86 of cell types.

87 **IAV and SARS-CoV-2 co-infection in mice results in increased SARS-CoV-2 viral**  
88 **load and more severe lung damage.**

89 The hACE2 transgenic mice were applied to study the interaction between IAV and  
90 SARS-CoV-2 *in vivo*. Mice were infected with  $3 \times 10^5$  PFU of SARS-CoV-2 with or without  
91 2000 PFU of IAV pre-infection and were then sacrificed two days later after SARS-CoV-2  
92 infection (the experimental scheme is shown in Fig. 2A). The viral RNA genome copies  
93 from lung homogenates confirmed that SARS-CoV-2 efficiently infected both groups  
94 (more than  $4 \times 10^8$  N gene copies) (Fig. 2B), while the influenza NP gene was only detected  
95 in IAV pre-infection group (Fig. 2B). Intriguingly, a significant increase in SARS-CoV-2  
96 viral load (12.9-fold increase in E gene and 6.6-fold increase in N gene) was observed in  
97 lung homogenates from co-infection mice compared to that from SARS-CoV-2 single-  
98 infected mice (Fig. 2C). The histological data in Fig. 2D further illustrated that IAV and  
99 SARS-CoV-2 co-infection induced more severe lung pathologic changes with massive  
100 infiltrating cells and obvious alveolar necrosis as compared to SARS-CoV-2 single  
101 infection or mock infection.

102 **IAV components specifically facilitate the entry process of SARS-CoV-2.**

103 We further tested if several other viruses on hand had similar effects to promote SARS-

104 CoV-2 infection. To our surprise, neither Sendai virus (SeV) (Fig. 3A), human rhinovirus  
105 (HRV3) (Fig. 3B), human parainfluenza virus (HPIV) (Fig. 3C), human respiratory  
106 syncytial virus (HRSV) (Fig. 3C) nor human enterovirus 71 (EV71) (Fig. 3C) could  
107 stimulate SARS-CoV-2 infection.

108 To explore how IAV promotes SARS-CoV-2 infection, we transfected A549 cells with  
109 eight individual viral genome segments of IAV to test if any of them could promote SARS-  
110 CoV-2 infectivity. The data in Fig. 3D and Fig. 3E showed that IAV segment-2 expression  
111 strongly stimulated SARS-CoV-2 multiplication in both SARS-CoV-2-infected cell lysates  
112 and supernatant.

### 113 **IAV infection induces elevated ACE2 expression.**

114 As IAV strongly increased the pseudotyped SARS-CoV-2 infection, we examined the  
115 viral entry process. It was reported that the cellular receptor angiotensin-converting  
116 enzyme 2 (ACE2)(13, 14), together with transmembrane serine protease 2 (TMPRSS2)  
117 (15), Furin(16) and cathepsin L (CatL)(17, 18), mediated SARS-CoV-2 viral entry. In IAV-  
118 infected cells, we found that the mRNA level of ACE2 and TMPRSS2, but not Furin and  
119 CatL were increased around three folds (A549 in Fig. 4A, Calu-3 in Fig. S2). An obvious  
120 switch of intracellular ACE2 expression was triggered at 12 h post-IAV-infection (Fig. 4C).  
121 In the meantime, influenza NP, Mx1, and ISG54 increased accordingly confirming a  
122 successful infection of IAV (Fig. 4B).

123 Interestingly, ACE2 mRNA level increased more dramatically in IAV and SARS-CoV-2  
124 co-infection cells with 28 folds in A549 (Fig. 4D), 5 folds in Calu-3 (Fig. 4E), 6 folds in

125 NHBE (Fig. 4F) respectively. The mRNA and protein levels (Fig. 4G) of ACE2 also  
126 increased accordingly in lung homogenates from co-infection mice.

127 When the cell mixture was transduced by lentivirus coding ACE2-sgRNA to knockdown  
128 ACE2 expression (Fig. 4H), the IAV-mediated enhancement of SARS-CoV-2 infection was  
129 totally abolished (Fig. 4I). Consist of this, ACE2 mRNA levels increased 13.8-fold in  
130 SARS-CoV-2-infected cells expressing segment-2 compared to that in control cells  
131 transfected with vector (Fig. 4J). Again, the enhanced SARS-CoV-2 infectivity mediated  
132 by segment-2 could be blocked in ACE2 knock-down cells (Fig. 4K).

133 The data indicated that IAV permitted increased SARS-CoV-2 infection through the up-  
134 regulation of ACE2 expression.

### 135 **Enhanced SARS-CoV-2 infectivity is independent of IFN signaling.**

136 ACE2 was reported to be an interferon-stimulated gene (ISG) in human airway epithelial  
137 cells(19). IAV infection will also stimulate type I IFN signaling. We, therefore, tested  
138 whether the augment of ACE2 expression is dependent on IFN or not. For this, cells were  
139 firstly pre-treated with different doses of IFN $\alpha$  (Fig. 5) and IFN $\gamma$  (Fig. S3 A-C) and then  
140 infected with pSARS-CoV-2. The data showed that IFN $\alpha$  could not promote the pSARS-  
141 CoV-2 infectivity in A549 cells (Fig. 5A), but rather significantly inhibit pSARS-CoV-2  
142 infectivity in Calu-3 (Fig. 5D) and Huh-7 (Fig. 5G) cells. Compared with the mRNA levels  
143 of ISG54 (Fig. 5 B, E, H), the mRNA levels of ACE2 and TMPRSS2 were only mildly  
144 increased around 1-3 folds under IFN treatment (Fig. 5 C, F, I). The data indicated that  
145 ACE2 could not robustly respond to IFN in these cells, which in turn suggested that ACE2

146 mediated viral entry was not affected by IFN.

147 Moreover, in IFNAR<sup>-/-</sup> A549 cells, the enhanced infectivity of pSARS-CoV-2 under IAV  
148 co-infection remained (Fig. 5J). By contrast to the decreased levels of ISG54 in IFNAR<sup>-/-</sup>  
149 A549 cells (Fig. S3D and Fig. 5K), the mRNA levels of ACE2 and TMPRSS2 still  
150 increased in IFNAR<sup>-/-</sup> A549 cells under IAV infection (Fig. 5L). The results strongly  
151 suggested that SARS-CoV-2 responded to IAV infection rather than IFN signaling for a  
152 favorable viral infection.

## 153 **Discussion**

154       Recently, there are many discussions about the possible impacts of the upcoming flu  
155 season on the current COVID-19 pandemic. Speculations have been raised that infection  
156 of IAV could induce more severe disease for the secondary SARS-CoV-2 infection, or co-  
157 infection of these two viruses cause more serious illness. However, no experimental data  
158 are available to show the relationship between IAV and SARS-CoV-2 yet. In this study, we  
159 provide the first experimental evidence that the pre-infection of IAV strongly promotes  
160 SARS-CoV-2 virus entry and infectivity in co-infected cells and animals. It emphasizes  
161 that influenza prevention during the SARS-CoV-2 pandemic season is of great importance.

162       Co-infection of viruses frequently occurs in nature. Some studies showed positive  
163 interaction between the dengue virus and the Zika virus via antibody-dependent  
164 enhancement(20). Other studies showed negative interactions between the common cold  
165 virus and SARS-CoV-2 via pre-existing immunity(21). By co-infection with IAV and  
166 pseudotyped or live SARS-CoV-2, we observed a great enhancement of SARS-CoV-2  
167 infectivity both in cell culture and *in vivo* in infected mice. Such enhancement was  
168 associated with the increased expression level of ACE2 which is a major receptor for  
169 SARS-CoV-2 to enter a host cell. We detected a 2-3 folds increase in ACE2 mRNA level  
170 post-IAV-infection (A549 cells). However, a much higher increase (28 folds) in the ACE2  
171 mRNA level could be detected under IAV and SARS-CoV-2 co-infection. We suspected  
172 that IAV infection induced a mild expression of ACE2 to permit SARS-CoV-2 virus entry  
173 so that the subsequent multiplication of SARS-CoV-2 would further enhance ACE2

174 expression in a positive feedback pattern(19).

175 Intriguingly, among all the viruses tested on hand, only IAV but not SeV, HRV3, HPIV,  
176 HRSV, or EV71 promoted SARS-CoV-2 infection. The three viruses of HRV3, HPIV, and  
177 HRSV are all prevalent pathogens to cause common cold in humans but had no effects on  
178 SARS-CoV-2 infectivity. EV71 is a major causative agent for hand-foot-and-mouth disease  
179 in young children, but again had little influence on SARS-CoV-2 infection. Furthermore,  
180 we confirmed the effects of IAV by H1N1 and H3N2 natural isolates (Fig. S4A), and the  
181 infectivity of the current D614G mutant SARS-CoV-2 can also be stimulated by IAV pre-  
182 infection (Fig. S4B). The unique feature for IAV to augment SARS-CoV-2 infectivity  
183 indicates that the influenza virus is the key pathogen of prevention and control during the  
184 current coronavirus pandemic.

185 Among the eight segments of IAV, segment-2 encoding PB1 promotes ACE2 expression  
186 and SARS-CoV-2 infectivity at the highest level. The detailed molecular mechanism  
187 underlying PB1 mediated SARS-CoV-2 enhancement needs further study. Nevertheless,  
188 the IAV PB1 segment encodes multiple viral proteins including PB1, PB1-F2, PB1-N40 to  
189 modulate host cells(22). PB1-F2 is a pro-apoptotic factor and can regulate innate  
190 immunity(23). PB1-N40 interacts with many host factors and contributes to viral  
191 pathogenicity(24). After all, the fact that the IAV PB1 segment could promote SARS-CoV-  
192 2 infection further confirms a unique positive interaction between IAV and SARS-CoV-2.

193 Importantly, the enhancement phenotype in IAV and SARS-CoV-2 co-infection is  
194 independent of IFN signaling. Therefore, influenza vaccination should be recommended to

195 people under the high risk of co-infection. Our findings remind the society that surveillance  
196 of co-infection is encouraged in the coming winter. And for sure, social distance and mask-  
197 wearing are beneficial to protect people from attacks of either or both the influenza virus.

198 **Methods**

199 **Cells and viruses.**

200 The 293T, A549, Huh-7, MDCK, and Vero E6, WI-38, WI-38 VA-13, and BEAS-2B were  
201 obtained from ATCC and maintained in Dulbecco's modified Eagle's medium (DMEM;  
202 Gibco) supplemented with 10% foetal bovine serum (FBS), Calu-3 (ATCC) was  
203 maintained in DMEM supplemented with 20% FBS. NCI-H292(ATCC) was maintained  
204 with RPMI-1640 (Gibco) supplemented with 20% FBS. Normal Human Bronchial  
205 Epithelial cells (NHBE) cells (ATCC) were maintained in airway epithelial cell basal  
206 medium (ATCC PCS300030) supplemented with Bronchial/Tracheal  
207 Epithelial Cell Growth Kit (ATCC PCS-300-040). All cells were incubated at 37 °C, 5%  
208 CO<sub>2</sub>.

209 The A/WSN/33 virus was generated by reverse genetics as previously described(25).  
210 H1N1(A/Sichuan/01/2009) and H3N2 (A/Donghu/312/2006) were kindly provided by the  
211 Influenza Center in China CDC. Human rhinovirus (HRV3), human respiratory syncytial  
212 virus (HRSV), or human enterovirus 71 (EV71) were purchased from ATCC and stocked  
213 accordingly. The human parainfluenza virus (HPIV) was obtained from Prof. MingZhou  
214 Chen, Wuhan University. Sendai virus (SeV) was provided by Prof. Tianxian Li, Wuhan  
215 Institute of Virology. The SARS-CoV-2 live virus (strain IVCAS 6.7512) was provided by  
216 the National Virus Resource, Wuhan Institute of Virology, Chinese Academy of Sciences.

217 **Plasmids and transfection.**

218 The SARS-CoV-2-S-Δ18 expressing plasmid was a gift from Prof. Ningshao Xia, Xiamen

219 University. The eight WSN viral segments in pHW2000 plasmid were kindly provided by  
220 Prof. Hans Klenk, Marburg University. The DNA transfection reagent Fugene HD was  
221 purchased from Promega and the transfection was performed according to manuscript  
222 procedures.

### 223 **Pseudotype virus production.**

224 The pseudotyped VSV- $\Delta$ G viruses expressing either luciferase reporter or mCherry  
225 reporter were provided by Prof. Ningshao Xia, Xiamen University. To produce  
226 pseudotyped VSV- $\Delta$ G-Luc/mCherry bearing SARS-CoV-2 spike protein (pSARS-CoV-2),  
227 Vero E6 cells were seeded in 10 cm dish and transfected simultaneously with 15  $\mu$ g SARS-  
228 CoV-2-S- $\Delta$ 18 plasmid by Lipofectamine 3000 (Thermo). Forty-eight hours post-  
229 transfection, 150  $\mu$ l pseudotyped VSV- $\Delta$ G bearing VSV-G protein were used to infect Vero  
230 E6 cells. Cell supernatants were collected after another 24 hours clearing from cell debris  
231 by centrifugation at 3000rpm for 6 minutes, aliquoted and stored at  $-80^{\circ}\text{C}$ .

### 232 **Luciferase-based cell entry assay**

233 Target cells were seeded in 48-well plates and inoculated, in triplicate, with equivalent  
234 volumes of pseudotyped virus stocks with 1:5 dilution in DMEM (3% FBS) with or without  
235 IAV pre-infection. At 24 h post-pseudotype-infection, the luciferase activities were  
236 measured with the Luciferase Assay System (Promega E4550).

### 237 **Virus infection and IFN treatment**

238 For IAV infection, cells were washed with PBS and then incubated with viruses at different  
239 MOIs (from 0.01 to 1) in infection medium (DMEM, supplemented with 2% FBS, 1%

240 penicillin/streptomycin) at 37 °C, 5% CO<sub>2</sub>.

241 For SARS-CoV-2 infections, cells were incubated with SARS-CoV-2 live virus at MOI  
242 of 0.01 in infection medium (DMEM, 1% penicillin/streptomycin) and incubated at 37 °C,  
243 5% CO<sub>2</sub> for 1 hour with or without 12 h IAV pre-infection (MOI 0.1). Cells were then  
244 washed with PBS two times and then incubated in culture medium (DMEM, supplemented  
245 with 5% FBS, 1% penicillin/streptomycin) at 37 °C, 5% CO<sub>2</sub> for 48 hours.

246 For SeV, HRV3, HPIV, HRSV, or EV71 infection, cells were washed with PBS and then  
247 incubated with indicated viruses in infection medium (DMEM, supplemented with 3% FBS,  
248 1% penicillin/streptomycin) and incubated at 37 °C, 5% CO<sub>2</sub> for 12 hours.

249 For IFN treatment, recombinant human IFN $\alpha$  2a (Beyotime, P5646) and IFN $\gamma$  (Beyotime,  
250 P5664) were dissolved in 0.1% BSA and diluted in DMEM with 10% FBS, and then  
251 admitted to cells for 12 hours at indicated doses.

### 252 **Real-time reverse-transcriptase–polymerase chain reaction**

253 The mRNA levels of indicated genes were quantified by quantitative PCR with reverse  
254 transcription (qRT–PCR). Purified RNAs extracted by TRIzol (Invitrogen™,15596018)  
255 were subjected to reverse transcription with oligo dT primer (using Takara cat#RR037A  
256 Kit), and then the corresponding cDNAs were quantified using Hieff qPCR SYBR Green  
257 Master Mix (Yeason). Thermal cycling was performed in a 384-well reaction plate  
258 (ThermoFisher, 4343814). Gene-specific primers were shown in Supplementary Table 1.  
259 All the mRNA levels were normalized by  $\beta$ -actin in the same cell.

260 The relative number of SARS-CoV-2 viral genome copy number were determined using

261 Taqman RT-PCR Kit (Yeason). To acutely quantify the absolute number of SARS-CoV-2  
262 genome, a standard curve by measuring the SARS-CoV-2 N gene constructed in the pCMV-  
263 N plasmid was applied. All the SARS-CoV-2 genome copy numbers were normalized by  
264 GADPH in the same cell.

#### 265 **Western blot analysis.**

266 For western blots, cells were lysed in RIPA buffer on ice for 30 minutes and were separated  
267 by sodium dodecyl sulfate-polyacrylamide gel electrophoresis (SDS-PAGE) and subjected  
268 to western blot analysis. For mice experiments, half lung tissue from each mouse was  
269 homogenized in PBS followed by boiling in SDS lysis buffer (GE) at 100°C, 30 minutes.  
270 Rabbit monoclonal antibody against ACE2 (Abclonal, A4612, 1:1000), mouse monoclonal  
271 antibody against SARS-CoV Nucleoprotein (Sino Biological, 40143-MM05, 1:1000), anti-  
272 actin (Abclonal, 1:1000), were purchased commercially. The anti-influenza virus-NP was  
273 kindly provided by Prof. Ningshao. Xia. Peroxidase-conjugated secondary antibodies  
274 (Antgene, 1: 5000) were applied accordingly followed by image development with  
275 Chemiluminescent HRP Substrate Kit (Millipore Corporation).

#### 276 **Immunofluorescence**

277 A549 cells were fixed and incubated with primary antibodies. The primary antibodies used  
278 in this study were rabbit polyclonal antibody against ACE2 for immunofluorescence (Sino  
279 Biological, 10108-T26) and anti-influenza virus-NP (kindly provided by Prof. Ningshao  
280 Xia). The Alexa Fluor dye-conjugated secondary antibodies (Alexa Fluor R488, Invitrogen;  
281 Alexa Fluor M555, Invitrogen) and DAPI (Beyotime, C1002), were admitted afterward

282 according to standard protocols. Cell imaging was performed on a Leica TCS SP8 confocal  
283 laser scanning microscope (Leica).

#### 284 **ACE2 knocking-down cells**

285 Two sgRNAs targeting the hACE2 gene were designed under the protocol in  
286 <http://chopchop.cbu.uib.no> and commercially synthesized to clone in lenti-Cas9-blast  
287 vector (kindly provided by Prof. Hongbing Shu). The control sgRNA lentivirus construct  
288 was also provided by Prof. Hongbing Shu. In brief, A549 cells were plated at 6-well plates  
289 and transduced with lentivirus encoding CRISPR-Cas9 system including either ACE2  
290 sgRNA or control sgRNA. The cell mixtures were selected by blasticidin for one week to  
291 obtain ACE2 knocking-down cells. The gene knocking-down efficiencies were confirmed  
292 by measuring the ACE2 mRNA level through qRT-PCR analysis.

#### 293 **Mice**

294 The K18 hACE2 transgenic mice purchased from Gempharmatech were housed in ABSL-  
295 3 pathogen-free facilities under 12-h light-dark cycles with access to food and water. Mice  
296 were male, age-matched, and grouped for SARS-CoV-2 infection or IAV and SARS-CoV-  
297 2 co-infection. At day 0, mice were intranasally infected with PBS or 2000 PFU of WSN  
298 respectively, and then both groups were intranasally infected with  $3 \times 10^5$  PFU of SARS-  
299 CoV-2 at Day 2. Another two days later, mice were sacrificed to determine viral loads and  
300 submitted to histological assay.

#### 301 **Histology**

302 Lung tissue from infected mice was dissected at Day 2 post-SARS-CoV-2-infection, fixed,

303 and stained using a standard H&E procedure. The slides were scanned and analyzed by the  
304 Wuhan Sci-Meds company. The representative images from three mice in each group were  
305 shown.

### 306 **Statistical analysis**

307 If not indicated otherwise, Student's t-test was used for two-group comparisons. The \*p-  
308 value < 0.05, \*\*p-value < 0.01, \*\*\*p-value < 0.001 and \*\*\*\*p-value < 0.0001 were  
309 considered significant. Unless otherwise noted, error bars indicated as mean values with  
310 standard deviation of at least three biological experiments.

311 **References and Notes**

- 312 1. C. Huang *et al.*, Clinical features of patients infected with 2019 novel coronavirus in Wuhan, China.  
313 *The Lancet* **395**, 497-506 (2020).
- 314 2. C. Wang, P. W. Horby, F. G. Hayden, G. F. Gao, A novel coronavirus outbreak of global health  
315 concern. *The Lancet* **395**, 470-473 (2020).
- 316 3. D. van Riel *et al.*, Human and avian influenza viruses target different cells in the lower respiratory  
317 tract of humans and other mammals. **171**, 1215-1223 (2007).
- 318 4. A. St John, A. J. J. o. i. Rathore, Early Insights into Immune Responses during COVID-19. **205**,  
319 555-564 (2020).
- 320 5. Z. P. Traylor, F. Aeffner, I. C. J. I. Davis, O. R. Viruses, Influenza A H1N1 induces declines in  
321 alveolar gas exchange in mice consistent with rapid post-infection progression from acute lung  
322 injury to ARDS. **7**, (2013).
- 323 6. Y. Hou *et al.*, SARS-CoV-2 Reverse Genetics Reveals a Variable Infection Gradient in the  
324 Respiratory Tract. *Cell* **182**, (2020).
- 325 7. E. Belongia, M. J. S. Osterholm, COVID-19 and flu, a perfect storm. **368**, 1163 (2020).
- 326 8. Y. Liu *et al.*, Aerodynamic analysis of SARS-CoV-2 in two Wuhan hospitals. **582**, 557-560 (2020).
- 327 9. S. Olsen *et al.*, Decreased Influenza Activity During the COVID-19 Pandemic - United States,  
328 Australia, Chile, and South Africa, 2020. **69**, 1305-1309 (2020).
- 329 10. E. Cuadrado-Payán *et al.*, SARS-CoV-2 and influenza virus co-infection. *The Lancet* **395**, e84  
330 (2020).
- 331 11. X. Zheng *et al.*, Co-infection of SARS-CoV-2 and Influenza virus in Early Stage of the COVID-19

- 332 Epidemic in Wuhan, China. *Journal of Infection* **81**, e128-e129 (2020).
- 333 12. H. Kleine-Weber *et al.*, Mutations in the Spike Protein of Middle East Respiratory Syndrome  
334 Coronavirus Transmitted in Korea Increase Resistance to Antibody-Mediated Neutralization.  
335 *Journal of virology* **93**, e01381-01318 (2019).
- 336 13. Q. Wang *et al.*, Structural and Functional Basis of SARS-CoV-2 Entry by Using Human ACE2. **181**,  
337 894-904.e899 (2020).
- 338 14. J. Lan *et al.*, Structure of the SARS-CoV-2 spike receptor-binding domain bound to the ACE2  
339 receptor. **581**, 215-220 (2020).
- 340 15. M. Hoffmann *et al.*, SARS-CoV-2 Cell Entry Depends on ACE2 and TMPRSS2 and Is Blocked by  
341 a Clinically Proven Protease Inhibitor. *Cell* **181**, 271-280.e278 (2020).
- 342 16. C. Wu *et al.*, Furin, a potential therapeutic target for COVID-19. *iScience*, 101642 (2020).
- 343 17. C. Grimm, R. Tang, Could an endo-lysosomal ion channel be the Achilles heel of SARS-CoV2?  
344 *Cell Calcium* **88**, 102212 (2020).
- 345 18. A. C. Walls *et al.*, Structure, Function, and Antigenicity of the SARS-CoV-2 Spike Glycoprotein.  
346 *Cell* **181**, 281-292.e286 (2020).
- 347 19. C. G. K. Ziegler, S. J. Allon, S. K. Nyquist, I. M. Mbano, J. J. C. Ordovas-Montanes, SARS-CoV-2  
348 Receptor ACE2 Is an Interferon-Stimulated Gene in Human Airway Epithelial Cells and Is Detected  
349 in Specific Cell Subsets across Tissues. (2020).
- 350 20. L. Priyamvada, K. M. Quicke, W. H. Hudson, N. Onlamoon, J. J. P. N. A. U. S. A. Wrammert,  
351 Human antibody responses after dengue virus infection are highly cross-reactive to Zika virus. **113**,  
352 7852-7857 (2016).

- 353 21. J. Mateus *et al.*, Selective and cross-reactive SARS-CoV-2 T cell epitopes in unexposed humans.  
354 *Science*, (2020).
- 355 22. H. M. Wise *et al.*, A complicated message: Identification of a novel PB1-related protein translated  
356 from influenza A virus segment 2 mRNA. *Journal of virology* **83**, 8021-8031 (2009).
- 357 23. R. Wang *et al.*, Influenza A virus protein PB1-F2 impairs innate immunity by inducing mitophagy.  
358 1-16 (2020).
- 359 24. H. Wise *et al.*, Overlapping signals for translational regulation and packaging of influenza A virus  
360 segment 2. **39**, 7775-7790 (2011).
- 361 25. Q. Han *et al.*, Sumoylation of influenza A virus nucleoprotein is essential for intracellular trafficking  
362 and virus growth. **88**, 9379-9390 (2014).

363 **Acknowledgment**

364 **Funding:** This work was supported in part by the National Key Research and Development  
365 Program (grants 2018FYA0900801 to K.X., 2016YFA0502103 to K.L.), the National  
366 Natural Science Foundation of China (grants 31922004 and 81772202 to K.X.),  
367 Application & Frontier Research Program of the Wuhan Government (2019020701011463  
368 to K.X.), and Hubei Innovation Team Foundation (2020CFA015 to K.X. and K.L.).

369 **Author contributions:** K.X. and K.L. conceived the project and designed the experiments.  
370 L.B., J. D., M.G., X.W., Z. H., Z. Z., and YC. Z. coordinated the live SARS-CoV-2 study  
371 and performed animal infection experiments. YL. Z. and S. L. conducted pseudotyped virus  
372 infection experiments, IFN treatment experiments, and data analysis. L.B., J. D. solved the  
373 Immunofluorescence, Histopathologic and Immunohistochemical studies. X. L. performed  
374 SeV, HRV3, HPIV, HRSV, EV71 infection experiments. YL. Z and X. L. generated the  
375 mutant virus and performed the related test. L.B., S. L, J. D., and X. L. repeated the key  
376 experiments in infected cells. X. S., Q.L., D. N., M.X., K.S., J.Y., W.Z., Z. T., M. T., Y. Z.,  
377 C.S., M. D., L.Z., Y.C., and H.Y provided technical supports and the materials. L. D. carried  
378 out ACE2 knock-out cells and related analysis. K.X., K.L., S. L, and YL. Z wrote the  
379 manuscript with inputs from all the remaining authors. We also thank our group members  
380 of the SARS-CoV-2 working group in the State Key Laboratory of Virology, Wuhan  
381 University, who work tightly together during this new virus pandemic for their research  
382 spirits and courage. We are grateful to Taikang Insurance Group Co., Ltd, Beijing Taikang

383 Yicai Foundation, and Special Fund for COVID-19 Research of Wuhan University for their

384 great supports of this work.

385 **Competing interests:**

386 The authors declared there were no competing interests.

387 **Figure legends**

388 **Fig. 1. IAV promotes SARS-CoV-2 virus infectivity.** (A) Diagram of the experimental  
389 procedure. (B) A549 cells were infected with A/WSN/33 at indicated MOIs. At 6, 12, 24  
390 hours post-IAV-infection, cells were infected with pSARS-CoV-2 for another 24 hours.  
391 Luciferase activity was measured to reflect virus entry efficiency. P values are from  
392 unpaired One-way ANOVA. (C) A549 cells were infected with A/WSN/33 at MOI 0.1. At  
393 12 hours post-IAV-infection, cells were infected with VSV-G-Luc for another 24 hours.  
394 Luciferase activity was measured to reflect virus entry efficiency. (D) The indicated cells  
395 were infected with WSN at MOI 0.1. At 12 hours post-IAV-infection, cells were infected  
396 with pSARS-CoV-2 for another 24 hours. Luciferase activity was measured to reflect virus  
397 entry efficiency. (E) The experimental procedure of IAV and live SARS-CoV-2 co-  
398 infection. A549 (F), Calu-3 (G), and NHBE (H) cells were pre-infected with WSN at MOI  
399 0.1 for 12 hours. Cells were then infected with live SARS-CoV-2 at MOI 0.01 for another  
400 48 hours. Total RNA in cell lysates and the supernatant were collected to detect E and N  
401 gene by Taqman-qRT-PCR. The data were expressed as fold changes of viral RNA levels  
402 in IAV pre-infection cells relative to the non-IAV infection control. Values are mean  $\pm$  s.d.  
403 of three independent results. \* $P \leq 0.05$ , \*\* $P \leq 0.01$ , \*\*\* $P \leq 0.001$ , \*\*\*\* $P \leq 0.0001$ .

404 **Fig. 2. IAV and SARS-CoV-2 co-infection induce more severe pathology in infected**  
405 **mice.** (A) Diagram of the experimental procedure. K18 hACE2 transgene mice were firstly  
406 intranasally infected with 2000 PFU of WSN or PBS at Day 0. Two days post-IAV-infection,  
407 mice were intranasally infected with  $3 \times 10^5$  live SARS-CoV-2 or PBS. At day 4, half lung

408 tissues of all the mice were homogenized to detect RNA or protein levels. **(B)** The  
409 quantitative viral genome copy numbers of SARS-CoV-2 N **(B, left)** or IAV NP **(B, right)**  
410 were measured. **(C)** The relative mRNA levels of SARS-CoV-2 E **(C, left)**, N gene **(C,**  
411 **right)**, were measured from lung homogenates in indicated groups. The data were  
412 expressed as fold changes relative to the non-IAV infection control. **(D)** Histopathologic  
413 and immunohistochemical studies were performed with lung slide samples in indicated  
414 groups. **(B-D)** Values are mean  $\pm$  s.d. of three independent results. \* $P \leq 0.05$ , \*\* $P \leq 0.01$ ,  
415 \*\*\* $P \leq 0.001$ , \*\*\*\* $P \leq 0.0001$ .

416 **Fig. 3. The enhancement of SARS-CoV-2 infection especially responses to IAV. (A-C)**  
417 A549 cells were pre-infected with SeV, HRV3, HPIV, HRSV, or EV71 at indicated doses  
418 for 12 hours respectively. Cells were then infected with pSARS-CoV-2 for another 24 hours  
419 followed by measuring luciferase activity. **(D and E)** The eight individual segment of WSN  
420 were transfected to A549 cells 24 hours ahead of live SARS-CoV-2 infection. Total RNA  
421 was extracted from cell lysates **(D)** or supernatant **(E)** to detect the E gene by Taqman-qRT-  
422 PCR 48 hours-post-infection. The data were expressed as fold changes relative to the vector  
423 control. Values are mean  $\pm$  s.d. of three independent results. \* $P \leq 0.05$ , \*\* $P \leq 0.01$ ,  
424 \*\*\* $P \leq 0.001$ , \*\*\*\* $P \leq 0.0001$ .

425 **Fig. 4. ACE2 is essential for IAV to promote SARS-CoV-2 infection. (A and B)** A549  
426 cells were mock-infected or infected with WSN at MOI 0.1. At 12 hours post-infection  
427 (h.p.i.), total RNAs were extracted from cells, and mRNA of ACE2, TMPRSS2, Furin,  
428 CatL **(A)**, or mRNA of NP, Mx1, ISG54 **(B)** was evaluated by quantitative real-time PCR

429 (qRT-PCR) using SYBR green method. The data were expressed as fold changes relative  
430 to the Mock infections. (C) A549 cells were infected with WSN at MOI 0.1. IAV NP  
431 proteins (red) and ACE2 (green) were detected by an immunofluorescence assay using a  
432 confocal microscope at 12 hours-post-infection. Scale bars were shown. A549 (D), Calu-3  
433 (E), and NHBE (F) cells were pre-infected with WSN at MOI 0.1 for 12 hours. Cells were  
434 then infected with live SARS-CoV-2 at MOI 0.01 for another 48 hours. Total RNAs were  
435 extracted from cells and mRNA of ACE2 was evaluated by quantitative real-time PCR  
436 (qRT-PCR) using SYBR green method. The protein expression levels of ACE2, SARS-  
437 CoV-2 N gene, IAV NP, and  $\beta$ -actin were measured by western blot. (G) The relative  
438 mRNA levels of ACE2 were measured from lung homogenates in indicated groups and the  
439 protein expression of IAV NP and ACE2 were detected by western blot accordingly. (D-G  
440 and J) The data were expressed as fold changes relative to the non-IAV infection control.  
441 (H-K) To establish ACE2 knock-down cells, A549 cell mixture was transduced with  
442 lentivirus encoding CRISPR-Cas9 system with two guide RNAs targeting ACE2 (sgRNA1  
443 and sgRNA2) or control guide RNA respectively. Cells were infected with live SARS-CoV-  
444 2 at MOI 0.01 with or without IAV infection under the same procedure as above. The  
445 mRNA levels of ACE2 (qRT-PCR) (H) and SARS-CoV-2 E gene (Taqman-qRT-PCR) (I)  
446 expression were detected. (J) The mRNA level of ACE2 was detected by qRT-PCR in live  
447 SARS-CoV-2-infected cells transfected with either vector of WSN segment-2 respectively.  
448 (K) The mRNA levels of the SARS-CoV-2 E gene from either vector- or segment2-  
449 transfected cells were measured by Taqman-qRT-PCR at 48 hours post-live-SARS-CoV-2-

450 infection in the present of control sgRNA or ACE2 sgRNAs. The data were expressed as  
451 fold change relative to non-IAV infection control. Values are mean  $\pm$  s.d. of three  
452 independent results. \* $P \leq 0.05$ , \*\* $P \leq 0.01$ , \*\*\* $P \leq 0.001$ , \*\*\*\* $P \leq 0.0001$ .

453 **Fig. 5. Enhanced SARS-CoV-2 infection is independent of IFN signaling.** A549 (A, B,  
454 C), Calu-3 (D, E, F), and Huh-7 (G, H, I) cells were pre-treated with indicated doses of  
455 IFN $\alpha$  for 12 hours. Cells were then infected with pSARS-CoV-2 for another 24 hours  
456 followed by measuring luciferase activity and mRNA expression levels of indicated genes.  
457 The data of mRNA levels were expressed as fold changes relative to non-treatment cells.  
458 (J-L) WT A549, and IFNAR<sup>-/-</sup>A549 cells were infected with WSN at MOI 0.1 for 12 hours,  
459 cells were then infected with pSARS-CoV-2 for another 24 hours followed by measuring  
460 luciferase activity and mRNA expression levels of indicated genes. P values are from  
461 unpaired One-way ANOVA. Values are mean  $\pm$  s.d. of three independent results. \* $P \leq 0.05$ ,  
462 \*\* $P \leq 0.01$ , \*\*\* $P \leq 0.001$ , \*\*\*\* $P \leq 0.0001$ .

463 **Fig. S1 IAV facilitates the entry process of pSARS-CoV-2 (relate to Fig.1).**

464 A549 cells were infected with A/WSN/33 at indicated MOIs. At 12, 24 hours post-IAV-  
465 infection, cells were infected with pSARS-CoV-2 with mCherry reporter for another 24  
466 hours. Scale bars, 200  $\mu$ m.

467 **Fig. S2 IAV infection induces elevated ACE2 expression (relate to Fig.4).**

468 Calu-3 cells were mock-infected or infected with WSN at MOI of 0.1. At 12 hours h.p.i.,  
469 total RNAs were extracted from cells, and mRNA of ACE2, TMPRSS2, Furin, CatL, NP,  
470 Mx1, and ISG54 were evaluated by qRT-PCR using the SYBR green method. The data

471 were expressed as fold changes relative to the Mock infections. Values are mean  $\pm$  s.d. of  
472 three independent results. \* $P \leq 0.05$ , \*\* $P \leq 0.01$ , \*\*\* $P \leq 0.001$ , \*\*\*\* $P \leq 0.0001$ .

473 **Fig. S3 Enhanced SARS-CoV-2 infection is independent of IFN signaling (relate to**  
474 **Fig.5).**

475 A549 (A), Calu-3 (B), and Huh-7 (C) cells were pre-treated with indicated doses of IFN $\gamma$   
476 for 12 hours. Cells were then infected with pSARS-CoV-2 for another 24 hours followed  
477 by measuring luciferase activity. (D) WT, and IFNAR<sup>-/-</sup>A549 cells were treated with IFN $\alpha$   
478 at 1000 IU/mL for 12 hours, and the mRNA expression levels of indicated genes were  
479 measured. Values are mean  $\pm$  s.d. of three independent results. (A-C) P values are from  
480 unpaired One-way ANOVA. \* $P \leq 0.05$ , \*\* $P \leq 0.01$ , \*\*\* $P \leq 0.001$ , \*\*\*\* $P \leq 0.0001$ .

481 **Fig. S4 IAV facilitates viral entry of WT or mutant SARS-CoV-2.**

482 (A) MDCK cells were pre-infected with WSN (MOI=0.1), H1N1(MOI=1), or H3N2  
483 (MOI=1) for 12 hours and were then infected with pSARS-CoV-2 for another 24 hours  
484 followed by measuring luciferase activity. (B) A549 cells were pre-infected with WSN at  
485 MOI 0.1 for 12 hours and were then infected with D614G mutant pSARS-CoV-2 for  
486 another 24 hours followed by measuring luciferase activity. Values are mean  $\pm$  s.d. of three  
487 independent results. \* $P \leq 0.05$ , \*\* $P \leq 0.01$ , \*\*\* $P \leq 0.001$ .

Figure 1. IAV promotes SARS-CoV-2 virus infectivity.

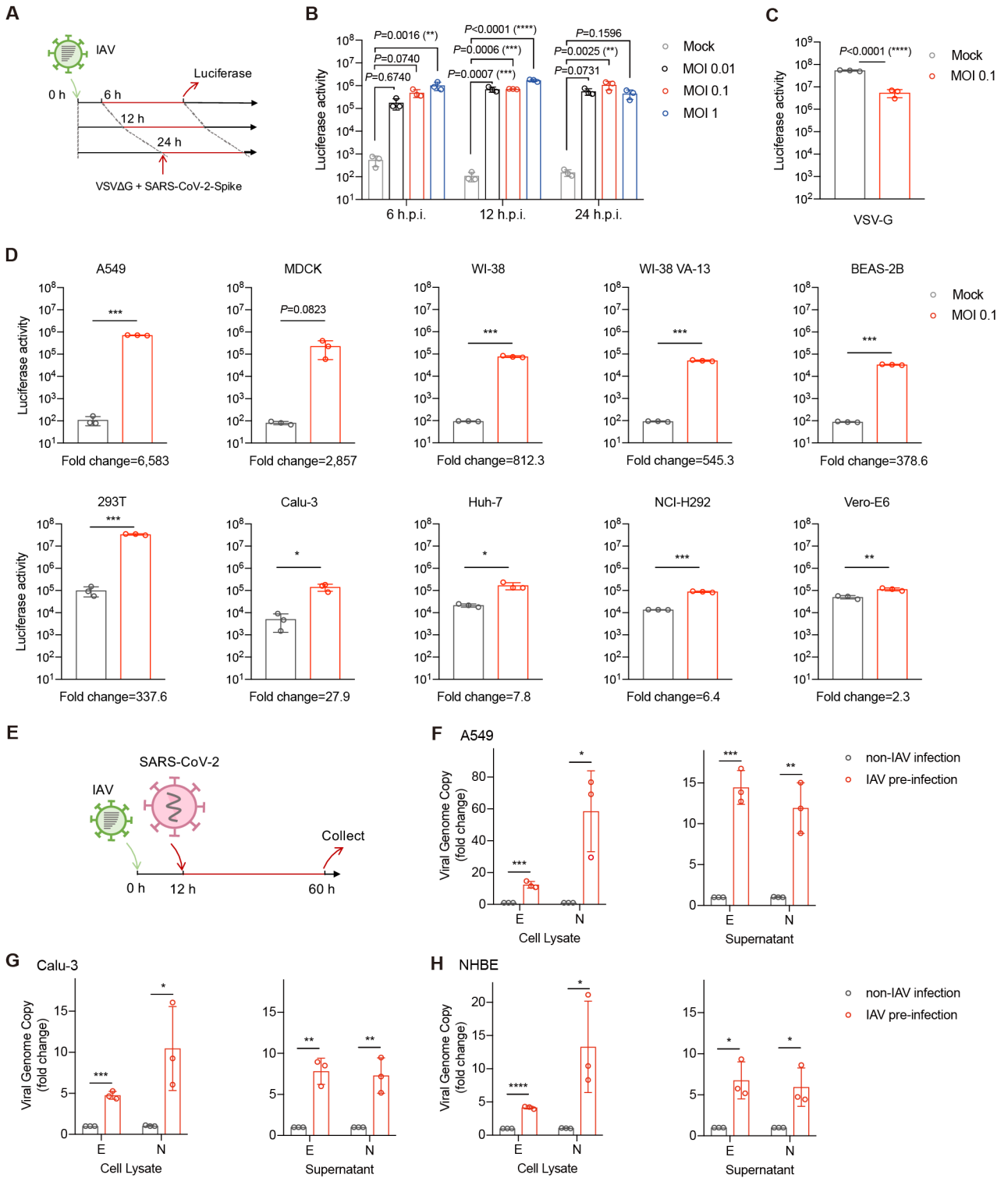


Figure 2. IAV and SARS-CoV-2 co-infection induces more severe pathology in infected mice.

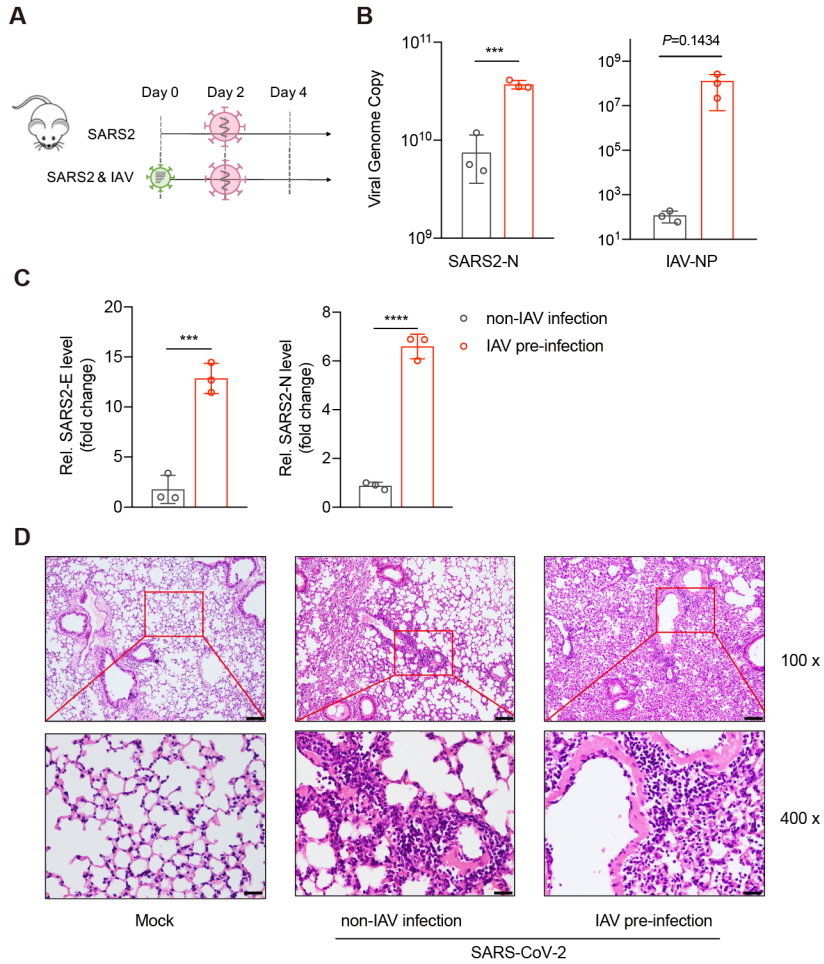


Figure 3. The enhancement of SARS-CoV-2 infection especially responses to IAV .

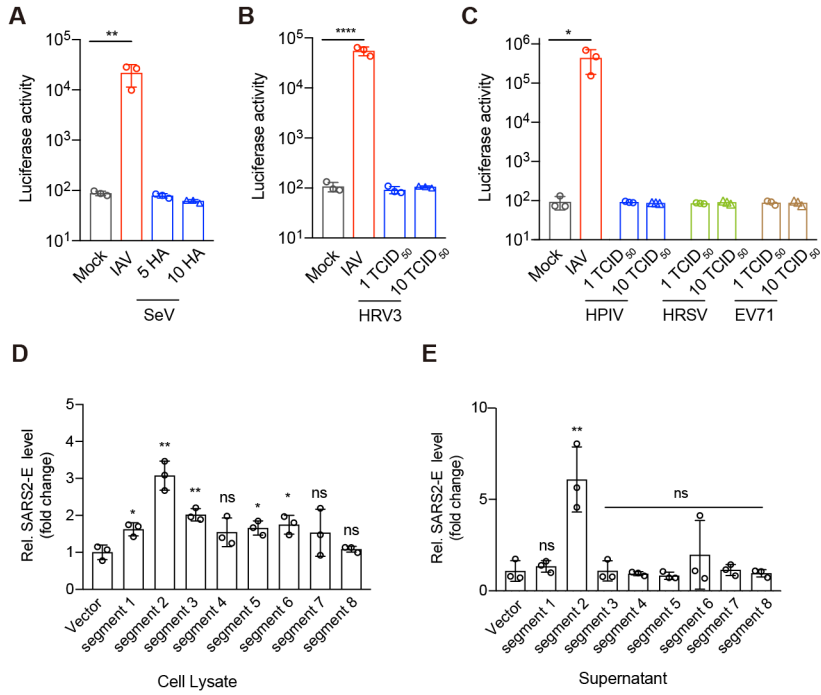


Figure 4. ACE2 is essential for IAV to promote SARS-CoV-2 infection.

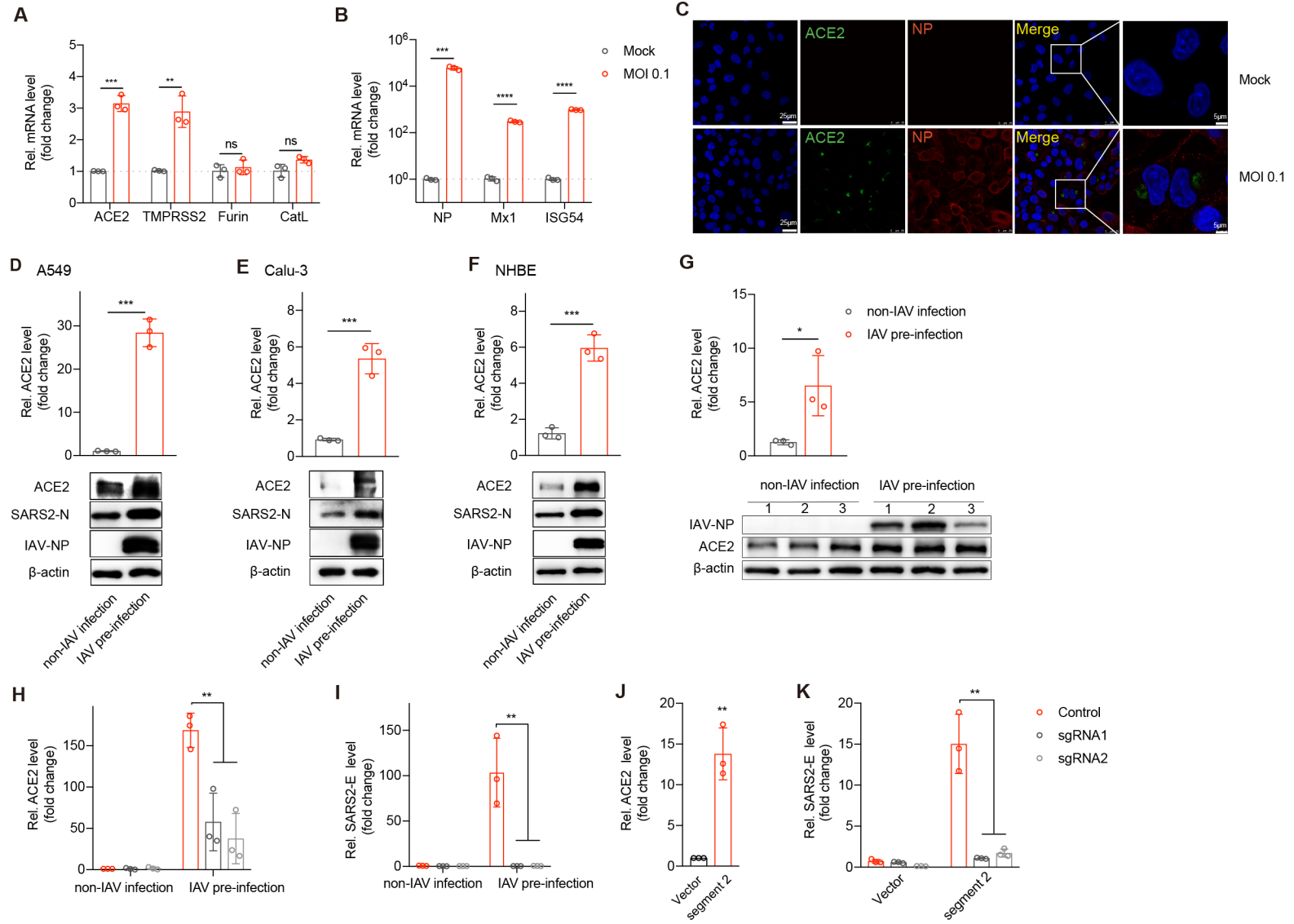


Figure 5. Enhanced SARS-CoV-2 infection is independent of IFN signaling.

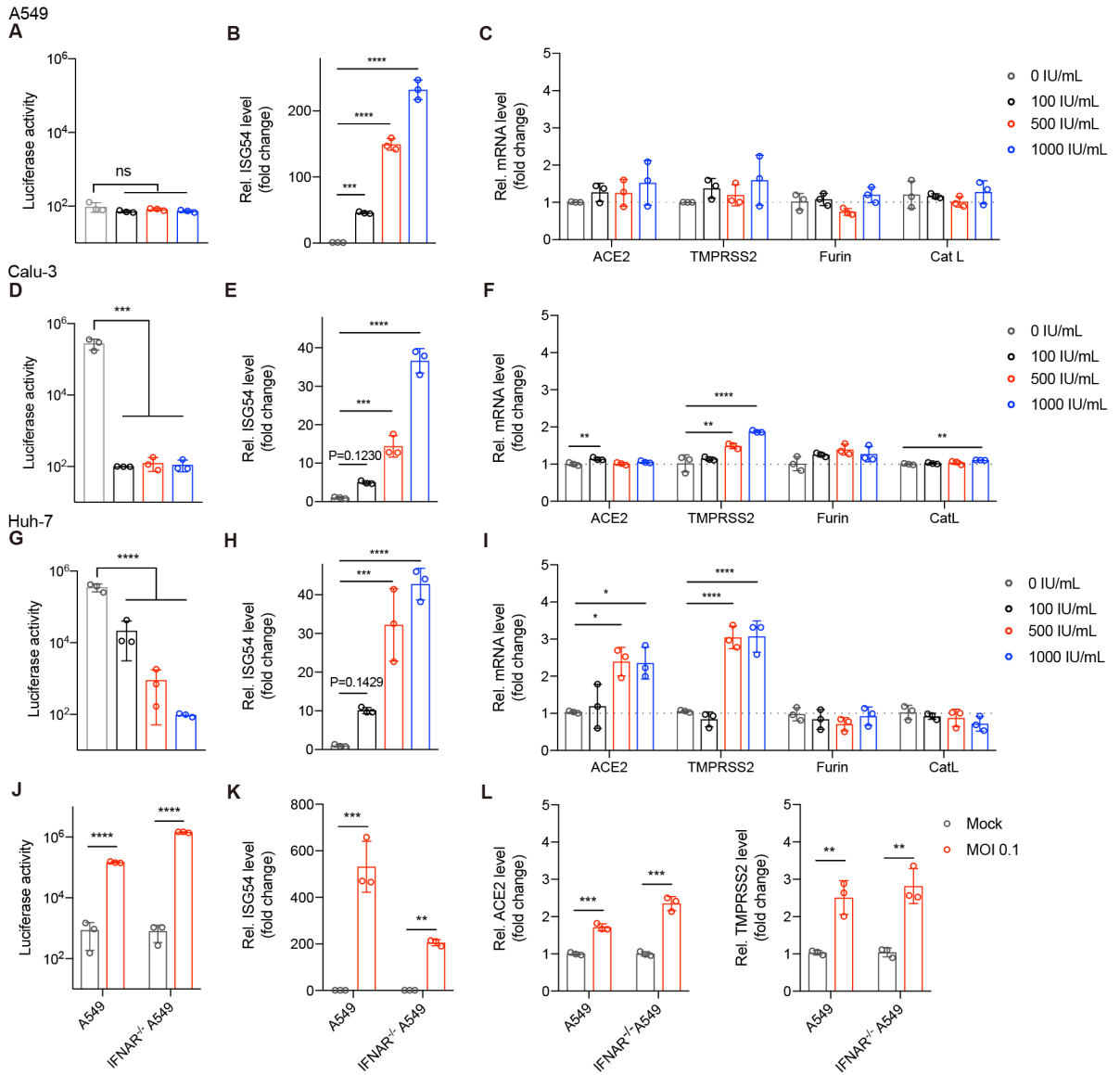


Figure S1. IAV facilitates the entry process of pSARS-CoV-2 (Fig.1).

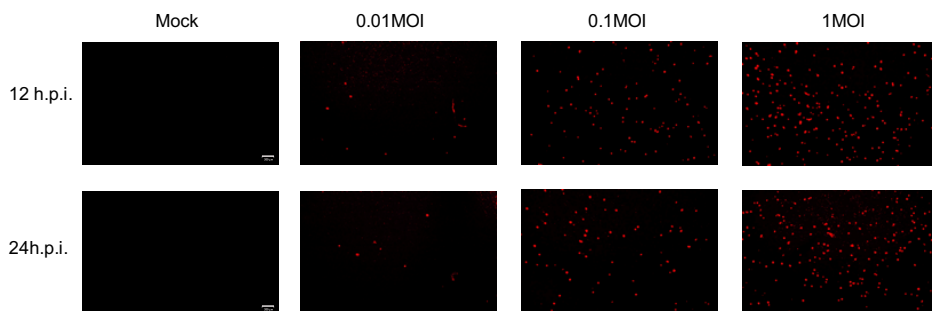


Figure S2. IAV infection induces elevated ACE2 expression (Fig.4).

Calu-3

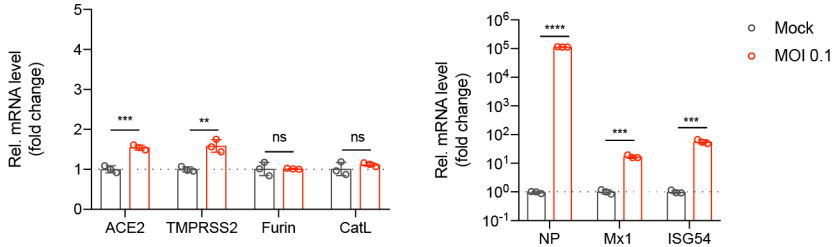


Figure S3. Enhanced SARS-CoV-2 infection is independent of IFN signaling (Fig.5).

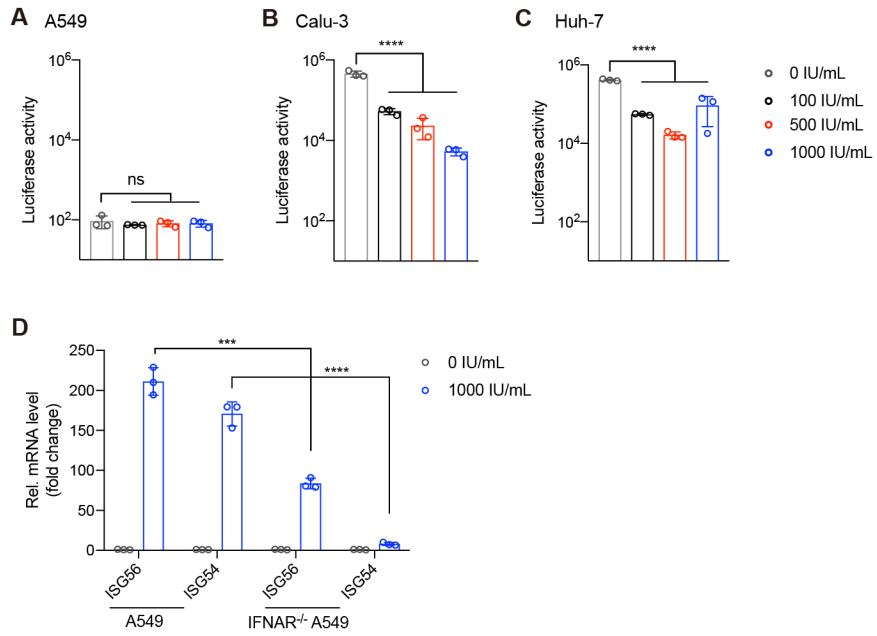
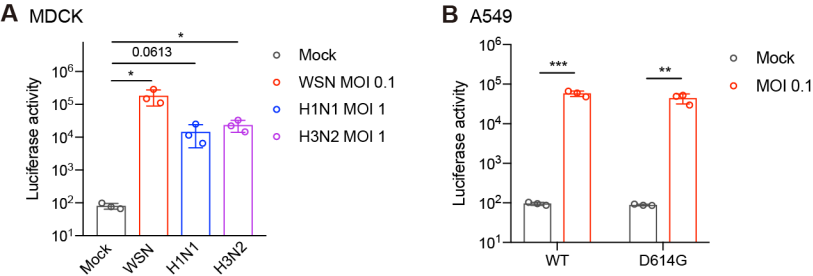


Figure S4. IAV facilitates viral entry of WT or mutant SARS-CoV-2.



Supplementary Table 1. Primers used in this paper.

Primer	Sequence (5'-3')
ACE2	CAAGAGCAAACGGTTGAACAC CCAGAGCCTCTCATTGTAGTCT
TMPRSS2	GCAGTGGTTTCTTTACGCTGT CCGCAAATGCCGTCCAATG
cathepsin L	TCGCGTCCTCAAGGCAATC CACAGTTGCGACTGCTTTCAT
Furin	GCAAAGCGACGGACTAAACG TGCCATCGTCCAGAATGGAGA
ISG54	CTGCAACCATGAGTGAGAA CCTTTGAGGTGCTTTAGATAG
ISG56	TACAGCAACCATGAGTACAA TCAGGTGTTTCACATAGGC
IAV NP-mRNA	GACTCACATGATGATCTGGCA CTTGTTCTCCGTCCATTCTCA
IAV NP-vRNA	AACGGCTGGTCTGACTCACATGAT AGTGAGCACATCCTGGGATCCATT
Mx1	GTTTCCGAAGTGGACATCGCA GTTTCCGAAGTGGACATCGCA
$\beta$ -actin	CATGTACGTTGCTATCCAGGC CATGTACGTTGCTATCCAGGC
SARS2-E	ACACTAGCCATCCTTACTGCGCTTCG
SARS2-N	GCAAATTGTGCAATTTGCGG
GAPDH	CTGCTTAGCACCCCTGGCCA